Transient Simulation of kp-Schrödinger Systems using Discrete Transparent Boundary Conditions

Andrea Zisowsky, Anton Arnold, Matthias Ehrhardt and Thomas Koprucki

Abstract This chapter is concerned with the derivation and analysis of discrete transparent boundary conditions (TBCs) for transient systems of *Schrödinger-type equations* in one space dimension. These systems occur i.e. in the physics of *layered semiconductor devices* as the so called $k \cdot p$-Schrödinger equations, which are a well established tool for *band structure calculations*.
The new TBCs are constructed directly for the chosen discrete scheme, in order to ensure the stability of the underlying scheme and to completely avoid any numerical reflections. The discrete TBCs are constructed using the solution of the exterior problem with Laplace and $\mathscr{Z}$-transformation, respectively.
These discrete TBCs can easily be obtained by an inverse $\mathscr{Z}$-transformation based on FFT, but these exact discrete TBCs are non-local in time and thus very costly. Hence, as a remedy, we present approximate discrete TBCs, that allow a fast calculation of the boundary terms using a sum-of-exponentials approach.

Andrea Zisowsky
Institut für Mathematik, Technische Universität Berlin, Strasse des 17. Juni 136, 10623 Berlin, e-mail: Andrea.Zisowsky@web.de

Anton Arnold
Institut für Analysis und Scientific Computing, Technische Universität Wien, Wiedner Hauptstr. 8, 1040 Wien, Austria, e-mail: anton.arnold@tuwien.ac.at

Matthias Ehrhardt
Lehrstuhl für Angewandte Mathematik und Numerische Analysis, Fachbereich C Mathematik und Naturwissenschaften, Bergische Universität Wuppertal, Gaußstr. 20, 42119 Wuppertal, Germany, e-mail: ehrhardt@math.uni-wuppertal.de

Thomas Koprucki
Weierstrass-Institut für Angewandte Analysis und Stochastik, Mohrenstrasse 39, 10117 Berlin, Germany, e-mail: koprucki@wias-berlin.de

1 Introduction

Many modern quantum-electronic semiconductor devices such as *resonant tunneling diodes* (RTD) [40, Chapter 14] or opto-electronic devices such as quantum-cascade lasers [41] and multi-quantum-well electro-absorption modulators [20] are based on the tunneling process of carriers through barrier structures. Typically these kind of barrier structures are *layered semiconductor heterostructures* [40, 41, 20] with a barrier thickness of a few nanometer. The transient simulation of wave packets tunneling through such nano-scale semiconductor heterostructures plays a key role in the understanding of such transport processes [48, 43, 39].

In this respect, transient simulations can be used to estimate charging and escape times [48, 43], tunneling times [39], or carrier life times [20, 46]. For the time-dependent simulation of a tunneling process usually a scalar Schrödinger equation defined by BenDaniel-Duke-type Hamiltonians [6, Chapter 3] is used [48, 39, 46]. Here the electronic band structure is approximated by a single parabolic band. These parabolic single-band approximations are in good agreement with the real band structure in the vicinity of the minima of the conduction bands, which is the part of the band structure that is usually occupied by the electrons. For the treatment of the holes, occupying the maxima of the valence bands, the accuracy of parabolic single-band models is often not sufficient since the valence bands possess a much more complex band structure [16, 6, 17, 19, 10, 39, 20].

However, the electronic states of the holes can be approximated appropriately by multi-band states which satisfy a so-called $k \cdot p$-Schrödinger equation. The time-dependent $k \cdot p$-Schrödinger equation describes the time evolution of the multi-band electronic state and can be regarded as a linear coupled system of scalar Schrödinger equations. The evolution is governed by the $k \cdot p$-Schrödinger operator which is an extension to the single-band models and describes a system of bands of the band structure, e.g. the four topmost valence bands [6, 17, 19, 10].

There exists a couple of such multi-band $k \cdot p$-models [36] including also combined models for conduction and valence bands. The later also allow for a non-parabolic approximation of the conduction bands. Such $k \cdot p$-models can be used for devices where the parabolic conduction band approximation is not sufficient. For unipolar devices where by crossing a barrier a conduction-band to valence-band transition is possible such as *resonant interband tunneling diodes* (RITD) or for bipolar devices where additionally the hole tunneling processes are important such as for multi-quantum well electro-absorption modulators multi-band modeling is necessary. In this cases the numerical solution of the transient $k \cdot p$-Schrödinger equation can be used to understand and to determine the tunneling properties of the corresponding semiconductor heterostructures by studying the time evolution of the multi-band electronic state.

In this chapter we discuss the appropriate numerical treatment of a transient system of $k \cdot p$-Schrödinger-type. We notice that such type of Schrödinger systems also arise as ”parabolic systems” in electromagnetic wave propagation. Artificial boundary conditions (BCs) have to be imposed to restrict the unbounded domain, on which the partial differential equation (PDE) is originally defined, to a finite computational

domain. Such BCs are called *transparent boundary conditions* (TBCs), if the solution on the whole space (restricted to the computational domain) is equal to the solution with the artificial BCs. The artificial boundary splits the problem into three parts: the interesting interior problem and a left and right exterior problem. For constant coefficients the exterior problems can be solved explicitly by the Laplace method in the continuous and $\mathscr{Z}$-transformation in the discrete case.

Claiming (spatial) C^1-continuity of the solution at the artificial boundaries yields the TBC as a Dirichlet–to–Neumann (DtN) map [2, 22]. An ad-hoc discretisation of these continuous TBC can destroy the stability of the employed numerical scheme for the PDE and induce numerical reflections [1]. To avoid this, we derive *discrete TBCs* for the fully discretised PDE. The procedure is analogous to the continuous case and uses the $\mathscr{Z}$-transformation. The inverse Laplace/$\mathscr{Z}$-transformation yields a convolution in time. Hence, the perfectly *exact* BC is non-local in time and therefore very costly for long–time simulations. To reduce the numerical effort, we introduce approximate discrete TBCs. Since the inverse $\mathscr{Z}$-transformation must be accomplished numerically for Schrödinger–type systems, an additional small numerical error is induced.

This chapter is organised as follows: In Section 2 we introduce the system of $k \cdot p$-Schrödinger equations and present as an example a quantum well structure with a double barrier that will be considered throughout this work. Next we derive in Section 3 the analytic TBC and afterwards its discrete variant in Section 4. Here, we also scrutinise the coefficients of the discrete convolution and explain our strategy to compute the coefficients by a numerical inverse $\mathscr{Z}$-transformation. In Section 5 we approximate the coefficients by a sum-of-exponentials ansatz and present a fast evaluation of the approximate discrete TBC. Finally, in Section 6 we give the results of numerical simulations for a quantum heterostructure.

2 Transient $k \cdot p$-Schrödinger Systems

In this chapter we consider $k \cdot p$-Schrödinger systems that are well established models for *band structure calculations* [18] for one-dimensional semiconductor nanostructures. They are layered *heterostructures* consisting of layers of different semiconductor materials with abrupt, planar heterojunction interfaces between the layers [40]. Typical examples are semiconductor quantum wells and double-barrier structures or *resonant interband tunneling diodes* (RITDs) [6, 19, 40, 44].

Fig. 1 depicts the typical valence and conduction band profile of a quantum well structure. Usually one is interested in the computation of the bound eigenstates (with eigenvalue smaller (large) than E_c (E_v) in the barrier material) in the quantum well. Here E_g denotes the bandgap and $e_{g'}$ is the middle of the bandgap that can be assumed to be constant on each material and thus as piecewise constant functions.

The typical valence and conduction band profile for a RITD is shown in Fig. 2. For the RITD one is usually interested in the computation of the transmission and

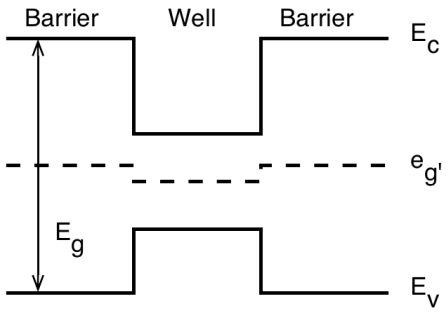

Fig. 1 Band edge profile for a quantum well structure. The electrons and holes are confined between the barriers in the well region.

reflection amplitudes in dependence on the wave vector of the incoming wave together with the corresponding wave functions.

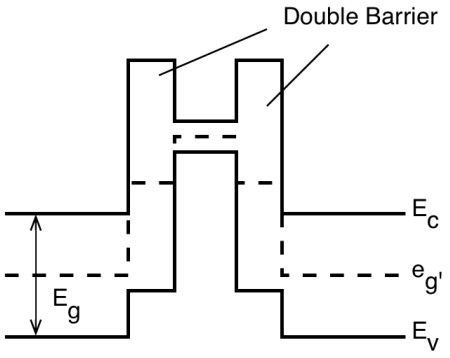

Fig. 2 Band edge profile for a RITD structure. By crossing from barrier to well region the electrons become a hole which is attracted by its potential well given by the valence band edge profile. This increases the density between the barriers and improves the performance of the tunneling device.

The $k\cdot p$-method [26] in combination with the envelope function approximation [6, 40, 19, 16, 6, 14, 15] is a frequently used approach for the modeling of the near-band-edge electronic states in semiconductor nanostructures. Within this approach the electronic state $\Psi(\mathbf{r})$ is approximated in terms of d bands

$$\Psi_{\mathbf{k}_\parallel}(\mathbf{r}) = \exp(i\mathbf{k}_\parallel\cdot\mathbf{r}_\parallel)\sum_{\nu=1}^{d}\varphi_\nu(x;\mathbf{k}_\parallel)u_{\nu,\mathbf{k}=\mathbf{0}}(\mathbf{r}) \qquad \text{with} \quad \mathbf{r}=(\mathbf{r}_\parallel,x)\in\mathbb{R}^3\,.$$

The index $\parallel$ indicates in-plane vectors and x denotes the growth direction of the semiconductor layers. $\mathbf{k}_\parallel=(k_1,k_2)\in\mathbb{R}^2$ is the reduced wave vector, which will be fixed for each simulation model. $u_{\nu,\mathbf{k}=\mathbf{0}}(\mathbf{r})$ are lattice periodic, zone-center Bloch functions varying on the atomic scale and $\varphi_\nu(x;\mathbf{k}_\parallel)$ are the corresponding envelope functions describing the variation of the wave function on the (larger) nanoscale. The vector of the envelope functions $\varphi=(\varphi_1,\cdots,\varphi_d)$ with $\varphi(x,t)\in\mathbb{C}^d$ fulfill the one-dimensional *$k\cdot p$-Schrödinger equation*

$$i\frac{\partial}{\partial t}\varphi = \mathbf{H}\Big(\mathbf{k}_{\|}, -i\frac{\partial}{\partial x}\Big)\varphi\,.$$

There is a hierarchy of $k\cdot p$-models [36] including 4-band, 6-band and 8-band Hamiltonians. Depending on the model Hamiltonian, effects such as quantum confinement, band-mixing, spin-orbit interaction and mechanical strain can be treated consistently. The basic stage in this model hierarchy is the 4×4 Luttinger-Kohn-Hamiltonian [35] which describes the band-mixing between the heavy holes and the light holes [6, 17, 18, 19].

In our notation we will follow Bandelow et al. [8] who performed a rigorous analysis of spectral properties for the spatially one dimensional $k\cdot p$-Schrödinger operators. The considered system reads as follows

$$\begin{aligned} i\frac{\partial}{\partial t}\varphi = &-\frac{\partial}{\partial x}(\mathbf{N}(x)\frac{\partial}{\partial x}\varphi) + \mathbf{M}_0(x)\frac{\partial}{\partial x}\varphi - \frac{\partial}{\partial x}(\mathbf{M}_0^H(x)\varphi)\\ &+k_1\left(\mathbf{M}_1(x)\frac{\partial}{\partial x}\varphi - \frac{\partial}{\partial x}(\mathbf{M}_1^H(x)\varphi)\right) + k_2\left(\mathbf{M}_2(x)\frac{\partial}{\partial x}\varphi - \frac{\partial}{\partial x}(\mathbf{M}_2^H(x)\varphi)\right)\\ &+k_1\mathbf{U}_1(x)\varphi + k_2\mathbf{U}_2(x)\varphi + k_1^2\mathbf{U}_{11}(x)\varphi + k_1k_2(\mathbf{U}_{12}(x)+\mathbf{U}_{21}(x))\varphi\\ &+k_2^2\mathbf{U}_{22}(x)\varphi + \mathbf{v}(x)\varphi + \mathbf{e}(x)\varphi, \qquad x\in\mathbb{R}, t>0, \quad k_1,k_2\in\mathbb{R}, \end{aligned} \tag{1}$$

where $\varphi(x,t)\in\mathbb{C}^d$, the mass matrix $\mathbf{N}$ and $\mathbf{e}$ are real diagonal $d\times d$-matrices. $\mathbf{U}_i$, $\mathbf{U}_{ij}$ and $\mathbf{v}$ are Hermitian $d\times d$-matrices. The $d\times d$-matrices $\mathbf{M}_0(x)$, $\mathbf{M}_1(x)$ and $\mathbf{M}_2(x)$ are skew-Hermitian. In the sequel we abbreviate

$$\mathbf{M}_S(x) := \mathbf{M}_0(x) + k_1\mathbf{M}_1(x) + k_2\mathbf{M}_2(x), \tag{2a}$$

$$\begin{aligned} \mathbf{V}(x) := &\, k_1\mathbf{U}_1(x) + k_2\mathbf{U}_2(x) + k_1^2\mathbf{U}_{11}(x) + k_2^2\mathbf{U}_{22}(x)\\ &+ k_1k_2(\mathbf{U}_{12}(x)+\mathbf{U}_{21}(x)) + \mathbf{v}(x) + \mathbf{e}(x). \end{aligned} \tag{2b}$$

Then $\mathbf{M}_S(x)$ is skew-Hermitian, $\mathbf{V}(x)$ is Hermitian and (1) reads

$$i\frac{\partial}{\partial t}\varphi = -\frac{\partial}{\partial x}(\mathbf{N}(x)\frac{\partial}{\partial x}\varphi) + \mathbf{M}_S(x)\frac{\partial}{\partial x}\varphi - \frac{\partial}{\partial x}(\mathbf{M}_S^H(x)\varphi) + \mathbf{V}(x)\varphi, \tag{3}$$

$x\in\mathbb{R}$, $t>0$. The real diagonal matrix $\mathbf{e}(x)$ describes the variation of the band-edges. The band-mixing due to the $k\cdot p$-interaction of the first and second order are described by the terms containing the matrices $\mathbf{M}_\alpha$, $\mathbf{U}_\alpha$, $\alpha=0,1,2$, and $\mathbf{U}_{\alpha\beta}$, $\alpha,\beta=1,2$, respectively. The potential $\mathbf{v}$ can cover couplings induced by the spin-orbit interaction or by mechanical strain. When neglecting all non-diagonal coupling terms, the system would reduce to an uncoupled system of scalar Schrödinger equations corresponding to the case of uncoupled parabolic bands. In this sense the couplings can be interpreted as correction terms to the parabolic band structure approximation.

An important property of the system (3) is the conservation of mass, i.e. $||\varphi||_{L^2}^2$ is constant in time. This property can be easily verified: we multiply (3) with φ^H from the left and integrate by parts:

$$\begin{aligned}\frac{\partial}{\partial t}||\varphi||_{L^2}^2 &= \frac{\partial}{\partial t}\int_{\mathbb{R}} \varphi^H \varphi \, dx = 2\,\mathrm{Im}\int_{\mathbb{R}} i\varphi^H \varphi_t \\ &= 2\,\mathrm{Im}\left(-\int_{\mathbb{R}} \varphi^H \frac{\partial}{\partial x}(\mathbf{m}\frac{\partial}{\partial x}\varphi)\,dx + \int_{\mathbb{R}} \varphi^H \mathbf{V}\varphi\,dx \right.\\ &\qquad \left. + \int_{\mathbb{R}} \varphi^H \mathbf{M}_S \frac{\partial}{\partial x}\varphi\,dx - \int_{\mathbb{R}} \varphi^H \frac{\partial}{\partial x}(\mathbf{M}_S^H \varphi)dx\right) \\ &= 2\,\mathrm{Im}\left(\int_{\mathbb{R}} \varphi_x^H \mathbf{m}\varphi_x\,dx + \int_{\mathbb{R}} \varphi^H \mathbf{V}\varphi\,dx + \int_{\mathbb{R}} \underbrace{\varphi^H \mathbf{M}\varphi_x + \varphi_x^H \mathbf{M}^H \varphi}_{\in\mathbb{R}}\,dx\right) \\ &= 0.\end{aligned}$$

The last equality follows from the fact that $\mathbf{V}$ and $\mathbf{N}$ are Hermitian and thus the imaginary part of the quadratic forms vanishes. The other term is of the form $y+y^H$ and thus obviously real.

We now briefly review an illustrative example from [50] that we will use throughout this chapter for the numerical results.

Example 1 (double-barrier stepped quantum-well structure [50]). We consider the GaAs/AlGaAs *double-barrier stepped quantum-well structure* (DBSQW) introduced in [48]. The variation of the band-edges $e(x)$ is depicted in Fig. 3. For this kind of structure an analysis of the time evolution of wave packets tunneling through the structure has been performed using a scalar Schrödinger equation [48]. We consider the more accurate four-band Luttinger-Kohn-Hamiltonian [6, 17, 18, 19] modeling the band-mixing of heavy and light holes. In atomic units adapted to the light holes ($\hbar = 1$, $m_0/(\gamma_1+2\gamma_2) = 1$) the coefficient matrices for the corresponding 4×4 system of Schrödinger equations are given by $\mathbf{N} = 0.5\cdot\mathrm{diag}(\gamma,1,1,\gamma)$, $\mathbf{M}_0 = \mathbf{0}$,

$$\mathbf{M}_1 = \frac{1}{2}\frac{\gamma_3}{\gamma_1+2\gamma_2}\sqrt{3}i\begin{pmatrix}0&1&0&0\\1&0&0&0\\0&0&0&-1\\0&0&-1&0\end{pmatrix}, \qquad \mathbf{M}_2 = \frac{1}{2}\frac{\gamma_3}{\gamma_1+2\gamma_2}\sqrt{3}\begin{pmatrix}0&1&0&0\\-1&0&0&0\\0&0&0&-1\\0&0&1&0\end{pmatrix},$$

$$\mathbf{U}_{11,22} = \frac{1}{2}\frac{1}{\gamma_1+2\gamma_2}\begin{pmatrix}\gamma_1+\gamma_2 & 0 & \mp\sqrt{3}\gamma_2 & 0\\ 0 & \gamma_1-\gamma_2 & 0 & \mp\sqrt{3}\gamma_2\\ \mp\sqrt{3}\gamma_2 & 0 & \gamma_1-\gamma_2 & 0\\ 0 & \mp\sqrt{3}\gamma_2 & 0 & \gamma_1+\gamma_2\end{pmatrix},$$

$$\mathbf{U}_{12}+\mathbf{U}_{21} = \frac{\sqrt{3}\gamma_3 i}{\gamma_1+2\gamma_2}\begin{pmatrix}0&0&1&0\\0&0&0&1\\-1&0&0&0\\0&-1&0&0\end{pmatrix},$$

and $\mathbf{U}_1 = \mathbf{U}_2 = \mathbf{0}$ with

$$\gamma = \frac{\gamma_1 - 2\gamma_2}{\gamma_1 + 2\gamma_2}.$$

The values of the band structure parameters for GaAs are given by

$$\gamma_1 = 6.85, \qquad \gamma_2 = 2.1, \qquad \gamma_3 = 2.9.$$

For the in-plane wave-vector $\mathbf{k}_{\|}$ we choose $k_1 = 2.3$, $k_2 = 0$. As initial condition we use a Gaussian wave packet

$$\varphi(x,0) = (2\pi\sigma^2)^{\frac{1}{4}} \exp\left(ik_r x - \frac{(x-x_0)^2}{\sigma^2} \right) \cdot \zeta\,, \tag{4}$$

where $\zeta \in \mathbb{C}^d$ is a linear combination of eigenmodes calculated via the dispersion relation of (3) and $\sigma = 3$, $x_0 = -2\sigma$ and $k_r = \sqrt{6.99}$. The band-edge profile $\mathbf{e}(x) = e(x)\mathbf{I}$ (with the identity matrix $\mathbf{I}$) of the DBSQW is taken from [48] and defined by

$$e(x) = \begin{cases} 0, & x \le 0 \\ \frac{15}{2}, & 0 < x \le 0.5 \\ \frac{3}{2}, & 0.5 < x \le 1 \\ 0, & 1 < x \le 1.5 \\ \frac{15}{2}, & 1.5 < x \le 2 \\ 0, & 2 < x \end{cases}. \tag{5}$$

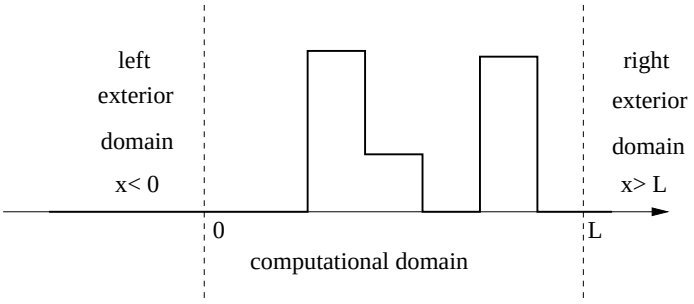

Fig. 3 Variation of the band-edge $e(x)$ for the GaAs/AlGaAs DBSQW structure.

The computational domain is now defined such that it contains the *significant* part of the initial data and the x-dependent part of the band-edge potential (cf. Fig. 3). For a strategy to soften this restriction on the inital data we refer the reader to [23]. Next we introduce in Section 3 TBCs at the left and right boundary $x = 0$ and $x = L$.

3 The Transparent Boundary Conditions

In this section we derive the TBCs for the $k \cdot p$-Schrödinger equation (1). In the scalar case (classical Schrödinger equation of quantum mechanics), the Laplace-transformed equation in the exterior domain can be solved explicitly. Afterwards the solution is inverse transformed, thus yielding the analytic boundary condition, cf. [2]. Here, for a system the inverse transform can not be calculated explicitly. Nevertheless, we will present the derivation of the Laplace transformed TBC.

For the derivation we proceed as follows: we consider the Schrödinger equation in the exterior domain. A Laplace transformation with respect to time yields a system of ordinary differential equations (ODEs), that can be reduced to first order. Then the solution of this system can be given in terms of its eigenvalues and eigenvectors. Next, we prove, that half of the eigenvalues have positive real parts and thus yield solutions increasing for $x \to \infty$; the other half has negative real parts, yielding decreasing solutions. Requiring that the part of the increasing solutions in the right (and the decreasing solutions in the left) exterior domain vanish, yields the TBC.

We consider equation (1) in the bounded domain $[0,L]$ supplied with TBCs at $x = 0$ and $x = L$. Since the derivation for the left and right TBC is analogous, we focus on the right boundary at $x = L$. The TBC at $x = L$ is constructed by considering (1) with constant coefficients for $x > L$, the so called *right exterior problem*

$$i\varphi_t = -\mathbf{N}\varphi_{xx} + i\mathbf{M}\varphi_x + \mathbf{V}\varphi, \qquad x > L,\ t > 0, \tag{6}$$

where $\mathbf{M} = \mathbf{M}^H$, $\mathbf{V} = \mathbf{V}^H$. $\mathbf{N}$ is diagonal, real and regular and given by

$$\begin{aligned}\mathbf{M} &= -i\left(\mathbf{M}_0 - \mathbf{M}_0^H + k_1(\mathbf{M}_1 - \mathbf{M}_1^H) + k_2(\mathbf{M}_2 - \mathbf{M}_2^H)\right)\\ &= -i(\mathbf{M}_S - \mathbf{M}_S^H), \qquad (7a)\\ \mathbf{V} &= k_1\mathbf{U}_1 + k_2\mathbf{U}_2 + k_1^2\mathbf{U}_{11} + k_2^2\mathbf{U}_{22} + k_1k_2(\mathbf{U}_{12} + \mathbf{U}_{21}) + \mathbf{v} + \mathbf{e}. \qquad (7b)\end{aligned}$$

If $\mathbf{M}_S$ is skew-Hermitian, then $\mathbf{M}_S - \mathbf{M}_S^H = 2\mathbf{M}_S$ is also skew-Hermitian, thus $\mathbf{M} = -2i\mathbf{M}_S$ is Hermitian. Analogously we define the *left exterior problem* for $x < 0$ and denote the occurring matrices with "$\tilde{}$".

To solve the right exterior problem for $x > L$ we apply the Laplace-transformation

$$\hat{\varphi}(x,s) = \int_0^\infty e^{-st}\varphi(x,t)\,dt, \quad s = \alpha + i\xi, \quad \alpha > 0, \quad \xi \in \mathbb{R}, \tag{8}$$

to (6) and obtain the system of ODEs

$$\mathbf{N}\hat{\varphi}_{xx} - i\mathbf{M}\hat{\varphi}_x = (\mathbf{V} - is\mathbf{I})\hat{\varphi}, \qquad x > L. \tag{9}$$

This transformed right exterior problem (9) posses a *unique classical solution*:

Lemma 1. *[50, Lemma 3.1] Let* $\mathrm{Re}(s) > 0$. *Then, the boundary value problem* (9) *with the boundary data*

$$\hat{\varphi}(x=L)=\hat{\Phi}\in\mathbb{C}^d,\qquad \hat{\varphi}(x=\infty)=0 \tag{10}$$

has a unique (classical) solution.

It is exactly this linear mapping from the boundary data to the (derivative of the) solution $\hat{\varphi}_L \mapsto \hat{\varphi}_x(L)$, the so-called Dirichet-to-Neumann (DtN) map, that represents the Laplace transformed TBC we are seeking for.

Next, to derive an explicit form of this TBC being accessible for numerical implementations, we define $\nu=\hat{\varphi}$ and $\eta=\hat{\varphi}_x$. Doing so, we reduce the order of the ODE and obtain a system of first order ODEs

$$\underbrace{\begin{pmatrix}\mathbf{M} & i\mathbf{N}\\ -i\mathbf{N} & \mathbf{0}\end{pmatrix}}_{\mathbf{A}}\begin{pmatrix}\nu_x\\ \eta_x\end{pmatrix}=\underbrace{\begin{pmatrix}i\mathbf{V}+s\mathbf{I} & \mathbf{0}\\ \mathbf{0} & -i\mathbf{N}\end{pmatrix}}_{\mathbf{B}}\begin{pmatrix}\nu\\ \eta\end{pmatrix},\qquad x>L. \tag{11}$$

In [50, Lemma 3.4] we proved the regularity of the matrix $\mathbf{A}^{-1}\mathbf{B}$ for $\mathrm{Re}(s)>0$ and thus we can rewrite (11) as

$$\begin{pmatrix}\nu_x\\ \eta_x\end{pmatrix}=\underbrace{\begin{pmatrix}\mathbf{0} & I\\ \mathbf{N}^{-1}(\mathbf{V}-is\mathbf{I}) & i\mathbf{N}^{-1}\mathbf{M}\end{pmatrix}}_{\mathbf{A}^{-1}\mathbf{B}}\begin{pmatrix}\nu\\ \eta\end{pmatrix},\qquad x>L. \tag{12}$$

In order to understand the structure of the solution we have to distinguish between increasing and decaying solutions of the system (12). For this purpose we proved using a continuity argument in [50] the Splitting Theorem:

Theorem 1. *[50, Theorem 3.2] The regular matrix $\mathbf{A}^{-1}\mathbf{B}$ has d eigenvalues with positive real part and d with negative real part.*

The next step is to transform $\mathbf{A}^{-1}\mathbf{B}$ in (12) to a Jordan form with

$$\mathbf{A}^{-1}\mathbf{B}=\mathbf{P}\mathbf{J}\mathbf{P}^{-1},$$

where $\mathbf{P}$ contains the left eigenvectors in columns. We sort the Jordan blocks in $\mathbf{J}$ with respect to an increasing real part of the corresponding eigenvalue. Thus $\mathbf{J}$ can be written as a block diagonal matrix $\mathbf{J}=\mathrm{diag}(\mathbf{J}_1,\mathbf{J}_2)$, where $\mathbf{J}_1$ holds all Jordan blocks to eigenvalues with negative real parts and $\mathbf{J}_2$ those with positive real parts. Due to the Splitting Theorem $\mathbf{J}_1$ and $\mathbf{J}_2$ are $d\times d$-matrices and equation (12) reads

$$\underbrace{\begin{pmatrix}\mathbf{P}_1 & \mathbf{P}_2\\ \mathbf{P}_3 & \mathbf{P}_4\end{pmatrix}}_{\mathbf{P}^{-1}}\begin{pmatrix}\nu_x\\ \eta_x\end{pmatrix}=\begin{pmatrix}\mathbf{J}_1 & 0\\ 0 & \mathbf{J}_2\end{pmatrix}\begin{pmatrix}\mathbf{P}_1\nu+\mathbf{P}_2\eta\\ \mathbf{P}_3\nu+\mathbf{P}_4\eta\end{pmatrix}. \tag{13}$$

Obviously, the upper part of this system yields parts of the solution, which decay for $x\to\infty$ and grow for $x\to-\infty$. The opposite is true for the lower part. An analogous equation holds for the left exterior problem. Thus the *transformed transparent boundary conditions* for the left (a) and right (b) boundary is obtained by extinguishing the respectively increasing parts of the exterior solutions:

$$\tilde{\mathbf{P}}_2\hat{\varphi}_x(0,s) = -\tilde{\mathbf{P}}_1\hat{\varphi}(0,s), \tag{14a}$$

$$\mathbf{P}_4\hat{\varphi}_x(L,s) = -\mathbf{P}_3\hat{\varphi}(L,s). \tag{14b}$$

Here, $\tilde{\mathbf{P}}_1$ and $\tilde{\mathbf{P}}_2$ are the corresponding matrices for the left exterior probem $\mathbf{P}_3$ and $\mathbf{P}_4$ (resp. $\tilde{\mathbf{P}}_1$,$\tilde{\mathbf{P}}_2$) are sub-matrices of $\mathbf{P}^{-1}$ which holds the eigenvectors of $\mathbf{A}^{-1}\mathbf{B}$ and is thus regular. Therefore $(\mathbf{P}_3 \quad \mathbf{P}_4)$ has rank d and thus at least one of the two matrices $\mathbf{P}_3$ and $\mathbf{P}_4$ (resp. $\tilde{\mathbf{P}}_1$ and $\tilde{\mathbf{P}}_2$) is regular. If the matrices $\tilde{\mathbf{P}}_2$ and $\mathbf{P}_4$ are regular, then the Laplace-transformed TBC can be written in *Dirichlet-to-Neumann form*. It is not clear, if these matrices are regular in general, but for our example this hold for all tested values of s.

4 The Discrete Transparent Boundary Conditions

Our proposed strategy is a purely discrete one, i.e. we do not discretise the equation (14) (by a numerical inverse Laplace transformation), but instead we derive discrete TBCs for a discretisation of (1). For the discretisation we choose a uniform grid with the step sizes h in space and k in time: $x_j = jh$, $t_n = nk$ with $j \in \mathbb{Z}$, $n \in \mathbb{N}_0$. We discretise (3) using the classical unitary Crank-Nicholson scheme in time and the central differences for the first and second spatial derivatives. The discrete $k \cdot p$-Schrödinger equation then reads

$$\begin{aligned} i\frac{h^2}{k}(\varphi_j^{n+1} - \varphi_j^n) \\ = -\Delta^0_{\frac{h}{2}}(\mathbf{N}_j\Delta^0_{\frac{h}{2}}\varphi_j^{n+\frac{1}{2}}) + \mathbf{M}_{Sj}\Delta^0\varphi_j^{n+\frac{1}{2}} - \Delta^0(\mathbf{M}_{Sj}^H\varphi_j^{n+\frac{1}{2}}) + V_j\varphi_j^{n+\frac{1}{2}}, \end{aligned} \tag{15}$$

with the centered difference operators

$$\Delta^0_{\frac{h}{2}}\varphi_j = \varphi_{j+\frac{1}{2}} - \varphi_{j-\frac{1}{2}}, \tag{16a}$$

$$\Delta^0\varphi_j = \frac{1}{2}(\Delta^+ + \Delta^-)\varphi_j = \varphi_{j+1} - \varphi_{j-1}, \tag{16b}$$

where $\Delta^+ = \varphi_{j+1} - \varphi_j$, $\Delta^- = \varphi_j - \varphi_{j-1}$ are the standard forward and backward differences and the arithmetic time average is denoted by $\varphi_j^{n+1/2} = (\varphi_j^{n+1} + \varphi_j^n)/2$.

An appropriate discretisation scheme should carry over properties of the continuous equation to the difference equation. This is the case for the Crank-Nicolson scheme: it conserves the discrete ℓ^2-norm on $j \in \mathbb{Z}$ and thus it is unconditionally stable for the whole space problem. The procedure to show this is analogue to the continuous case: we multiply the discrete equation with $(\varphi_j^n)^H$ from the left and add the Hermitian of the discrete equation multiplied by φ_j^{n+1} from the right. This shows, that the discrete ℓ^2-norm is conserved in time.

For the case of a scalar Schrödinger equation Arnold [2] derived 1998 a discrete TBC. This discrete TBC is reflection-free and conserves the stability properties of the whole-space Crank-Nicolson scheme. The discrete TBC has the form of a discrete convolution. The convolution coefficients are a function of Legendre polynomials but can be obtained more easily by a three-term recurrence formula. Ehrhardt and Arnold [22] showed that the imaginary parts of the convolution coefficients are not decaying and therefore introduced summed coefficients.

To derive the discrete TBC for a system of Schrödinger equations we solve the $\mathscr{Z}$-transformed system of ordinary difference equations (OΔEs) in the exterior domain. Then all its solutions are determined by eigenvalues and eigenvectors, which can distinguish between decaying and increasing solutions by the absolute value of the involved eigenvalue. We obtain the transformed discrete TBC by claiming, that no influence of increasing solutions exists.

In the exterior domain $j \geq J$ ($x_J = L$) the Crank-Nicholson scheme (15) simplifies

$$i\frac{h^2}{k}(\varphi_j^{n+1} - \varphi_j^n) = \\ -\mathbf{N}\Delta^+\Delta^-\varphi_j^{n+1/2} + ih\mathbf{M}\frac{1}{2}(\Delta^+ + \Delta^-)\varphi_j^{n+1/2} + h^2\mathbf{V}\varphi_j^{n+1/2}. \quad (17)$$

A $\mathscr{Z}$-transformation given by

$$\mathscr{Z}\{\varphi_j^n\} = \hat{\varphi}_j(z) := \sum_{n=0}^{\infty} z^{-n}\varphi_j^n, \qquad z \in \mathbb{C}, \qquad |z| > 1, \quad (18)$$

applied to (17) yields for $|z| > 1$ the system of second order OΔEs

$$2i\frac{h^2}{k}\frac{z-1}{z+1}\hat{\varphi}_j = -\mathbf{N}\Delta^+\Delta^-\hat{\varphi}_j + ih\mathbf{M}\frac{1}{2}(\Delta^+ + \Delta^-)\hat{\varphi}_j + h^2\mathbf{V}\hat{\varphi}_j, \qquad j \geq J. \quad (19)$$

As in the continuous case we proved in [50] that this transformed right exterior problem (19) posses a *unique solution*:

Lemma 2. *[50, Lemma 4.1] For each $z \in \mathbb{C}$ with $|z| > 1$ the $\mathscr{Z}$-transformed exterior problem* (19) *with the boundary data*

$$\hat{\varphi}_{J-1} = \hat{\Phi}, \qquad \hat{\varphi}_\infty = 0 \quad (20)$$

has a unique solution.

We proceed with the construction of the discrete TBC and define $\hat{\xi}_j = \Delta^-\hat{\varphi}_j$ in order to write (19) as a system of first order OΔEs

$$\underbrace{\begin{pmatrix} i\frac{h}{2}\mathbf{M} & -\mathbf{N} \\ -\mathbf{I} & \mathbf{I} \end{pmatrix}}_{\mathbf{A}} \begin{pmatrix} \Delta^+\hat{\varphi}_j \\ \Delta^+\hat{\xi}_j \end{pmatrix} = \underbrace{\begin{pmatrix} h^2 2\frac{z-1}{z+1}\frac{1}{k}i\mathbf{I} - h^2\mathbf{V} & -i\frac{h}{2}\mathbf{M} \\ \mathbf{0} & -\mathbf{I} \end{pmatrix}}_{\mathbf{B}} \begin{pmatrix} \hat{\varphi}_j \\ \hat{\xi}_j \end{pmatrix}, \qquad j \geq J \quad (21)$$

In [50, Lemma 4.5] we proved the regularity of the matrix $\mathbf{A}^{-1}\mathbf{B}+\mathbf{I}$ for $|z|\neq 1$ and thus we can rewrite (21) as

$$\begin{pmatrix}\hat{\varphi}_{j+1}\\ \hat{\xi}_{j+1}\end{pmatrix} = (\mathbf{A}^{-1}\mathbf{B}+\mathbf{I})\begin{pmatrix}\hat{\varphi}_j\\ \hat{\xi}_j\end{pmatrix}, \qquad j\geq J. \tag{22}$$

As in the continuous case there exist a discrete version of the Splitting Theorem:

Theorem 2. *[50, Theorem 4.2] For $|z|\neq 1$ d of the $2d$ eigenvalues of $\mathbf{A}^{-1}\mathbf{B}+\mathbf{I}$ have an absolute value strictly larger than 1 and d have an absolute value strictly smaller than 1.*

In other words, the eigenvalues $\lambda_1,\dots,\lambda_{2n}$ of $\mathbf{A}^{-1}\mathbf{B}$ split into two commensurate groups, i.e. the solutions involving those with $|\lambda_k+1|<1$ for $k=1,\dots,n$ decay for $j\to\infty$ and those with $|\lambda_k+1|>1$ for $k=n,\dots,2n$ decay for $j\to-\infty$.

Thus, as in the continuous case, we can split the Jordan form $\mathbf{J}=\operatorname{diag}(\mathbf{J}_1,\mathbf{J}_2)$ of $\mathbf{A}^{-1}\mathbf{B}$, $\mathbf{J}_1$ containing the Jordan blocks corresponding to solutions decaying for $j\to\infty$ and $\mathbf{J}_2$ those which increase. With the matrix of left eigenvectors $\mathbf{P}^{-1}$ the equation

$$\underbrace{\begin{pmatrix}\mathbf{P}_1 & \mathbf{P}_2\\ \mathbf{P}_3 & \mathbf{P}_4\end{pmatrix}}_{\mathbf{P}^{-1}}\begin{pmatrix}\Delta^+\hat{\varphi}_j\\ \Delta^+\hat{\xi}_j\end{pmatrix} = \mathbf{P}^{-1}\mathbf{A}^{-1}\mathbf{B}\begin{pmatrix}\hat{\varphi}_j\\ \hat{\xi}_j\end{pmatrix} = \begin{pmatrix}\mathbf{J}_1 & \mathbf{0}\\ \mathbf{0} & \mathbf{J}_2\end{pmatrix}\begin{pmatrix}\mathbf{P}_1\hat{\varphi}_j+\mathbf{P}_2\hat{\xi}_j\\ \mathbf{P}_3\hat{\varphi}_j+\mathbf{P}_4\hat{\xi}_j\end{pmatrix} \tag{23}$$

holds and the *transformed discrete TBCs* read

$$\tilde{\mathbf{P}}_1\hat{\varphi}_1+\tilde{\mathbf{P}}_2\hat{\xi}_1=0, \tag{24a}$$

$$\mathbf{P}_3\hat{\varphi}_J+\mathbf{P}_4\hat{\xi}_J=0, \tag{24b}$$

for the left (a) and right (b) boundary respectively. For nonsingular $\mathbf{P}_4$ and $\tilde{\mathbf{P}}_2$ (either $\mathbf{P}_4$ or $\mathbf{P}_3$ is regular, since their composition is a linear independent set of eigenvectors - the same holds for $\tilde{\mathbf{P}}_2$ and $\tilde{\mathbf{P}}_1$) and for $\widehat{\mathbf{D}}=-\mathbf{P}_4^{-1}\mathbf{P}_3$ and $\widehat{\tilde{\mathbf{D}}}=-\tilde{\mathbf{P}}_2^{-1}\tilde{\mathbf{P}}_1$ we write

$$\Delta^-\hat{\varphi}_1=\widehat{\tilde{\mathbf{D}}}\hat{\varphi}_1, \tag{25a}$$

$$\Delta^-\hat{\varphi}_J=\widehat{\mathbf{D}}\hat{\varphi}_J. \tag{25b}$$

After an inverse $\mathscr{Z}$-transformation the *discrete TBCs* read

$$\varphi_1^{n+1}-\varphi_0^{n+1}-\tilde{\mathbf{D}}^0\varphi_1^{n+1}=\sum_{k=1}^{n}\tilde{\mathbf{D}}^{n+1-k}\varphi_1^k, \tag{26a}$$

$$\varphi_J^{n+1}-\varphi_{J-1}^{n+1}-\mathbf{D}^0\varphi_J^{n+1}=\sum_{k=1}^{n}\mathbf{D}^{n+1-k}\varphi_J^k. \tag{26b}$$

We remark that in equation (25a) and (26a) the left boundary convolution is given at the interior grid point $j=1$. Of course, the boundary condition can also be formu-

lated at $j = 0$ using $\hat{\tilde{\xi}}_j = \Delta^+ \hat{\varphi}_j$. This changes the lower row in $\mathbf{A}$ and $\mathbf{B}$ and thus the matrix $\tilde{\mathbf{D}}$ differs from $\mathbf{D}$. Posing the boundary condition at $j = 1$ as we do, has the advantage, that these matrices coincide, if the coefficients for $x < 0$ and $x > L$ are equal, what occurs often in the application. In that case we can reduce the numerical effort to calculate the convolution coefficients by half.

For a scalar Schrödinger equation Ehrhardt and Arnold showed in [22] that the imaginary parts of the coefficients were not decaying but oscillating. As a remedy they introduced *summed coefficients* that decay rapidly like $O(n^{-3/2})$. Since the scalar equation is as a special case included in our system, it suggests itself to use the summed coefficients, although we cannot give any proof of the asymptotic behaviour of the systems' coefficients.

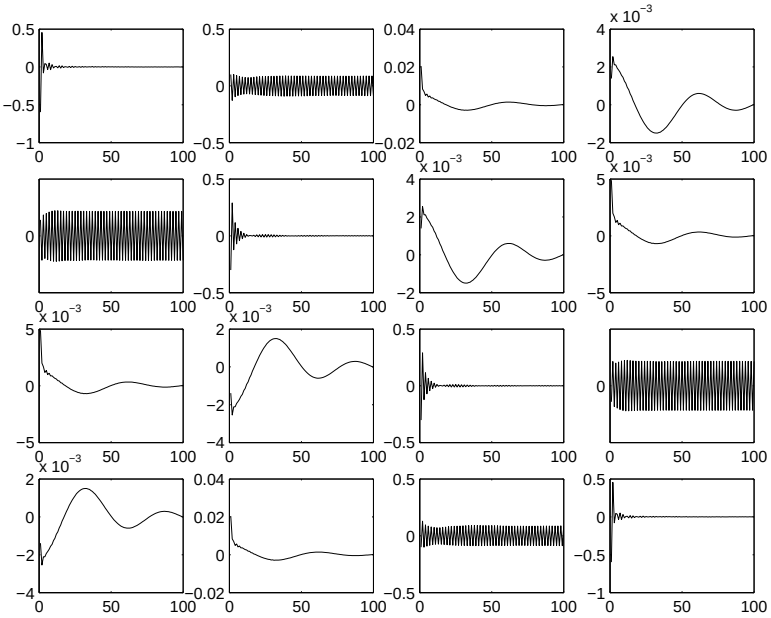

Fig. 4 Real parts of the convolution coefficients $\mathbf{D}^n_{k,l}$

In the Figs. 4–7 we plot typical examples of the numerically calculated coefficients for a 4×4 system. Especially in Fig. 5 one can observe in the diagonal elements the typical oscillating beaviour known from the scalar case. The diagonal elements show the same properties as those for the scalar case. For the summed coefficients

$$\widehat{\tilde{\mathbf{S}}}_{s,l} = \frac{z+1}{z}\widehat{\tilde{\mathbf{D}}}_{s,l} \qquad \text{and} \qquad \widehat{\mathbf{S}}_{s,l} = \frac{z+1}{z}\widehat{\mathbf{D}}_{s,l} \tag{27}$$

the boundary conditions read

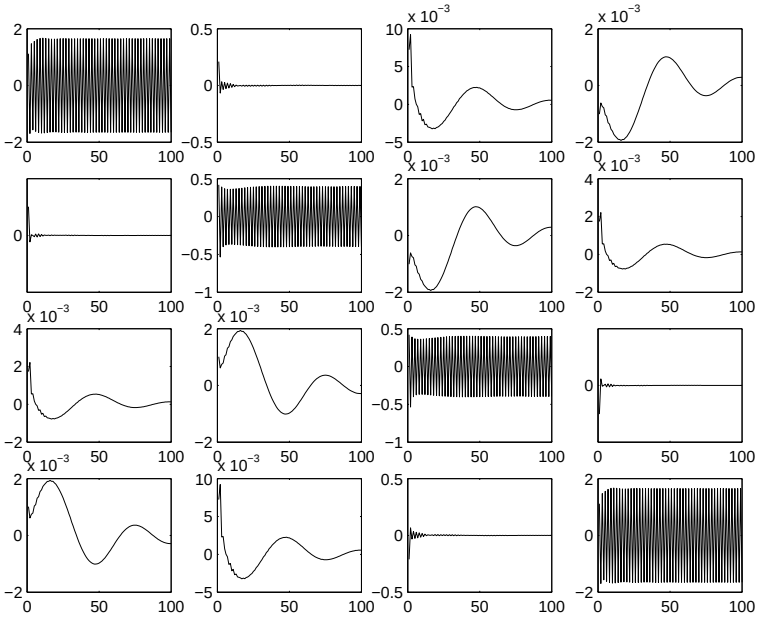

Fig. 5 Imaginary parts of the convolution coefficients $\mathbf{D}^n_{k,l}$

$$\varphi_1^{n+1} - \varphi_0^{n+1} - \tilde{\mathbf{S}}^0 \varphi_1^{n+1} = \sum_{k=1}^{n} \tilde{\mathbf{S}}^{n+1-k} \varphi_1^k - \varphi_1^n + \varphi_0^n, \tag{28a}$$

$$\varphi_J^{n+1} - \varphi_{J-1}^{n+1} - \mathbf{S}^0 \varphi_J^{n+1} = \sum_{k=1}^{n} \mathbf{S}^{n+1-k} \varphi_J^k - \varphi_J^n + \varphi_{J-1}^n. \tag{28b}$$

In order to compute the convolution coefficients we need to inverse $\mathscr{Z}$-transform the transformed kernels. We assume that the $\mathscr{Z}$-transform (18) is analytic for $|z| > R \geq 0$. The coefficients are then recovered by

$$\ell_n = \frac{1}{2\pi i} \oint_{S_\rho} \hat{\ell}(z) z^{n-1} dz,$$

where S_ρ denotes the circle with radius $\rho > R$. With the substitution $z = \rho e^{i\varphi}$ we obtain

$$\ell_n = \frac{\rho^n}{2\pi} \int_0^{2\pi} \hat{\ell}\left(\rho\, e^{i\varphi}\right) e^{in\varphi} d\varphi\,. \tag{29}$$

For $\rho > 1$, the *amplification factors* ρ^n in (29) will be the reason for the numerical instabilities. On the other hand, $\rho = 1$ cannot be chosen either for the application to DTBCs, due to the poor regularity of $\widehat{\mathbf{D}}(z)$ on the unit circle. For the scalar Schrödinger equation, e.g., $\hat{d}(z)$ has two branch-points of type $\sqrt{z^2-1}$ (cf. [2, 22]), and hence too many quadrature points would be necessary for the numerical evaluation of (29). But $\hat{d}(z)$ is analytic for $|z| > 1$. So, one has to choose ρ as a

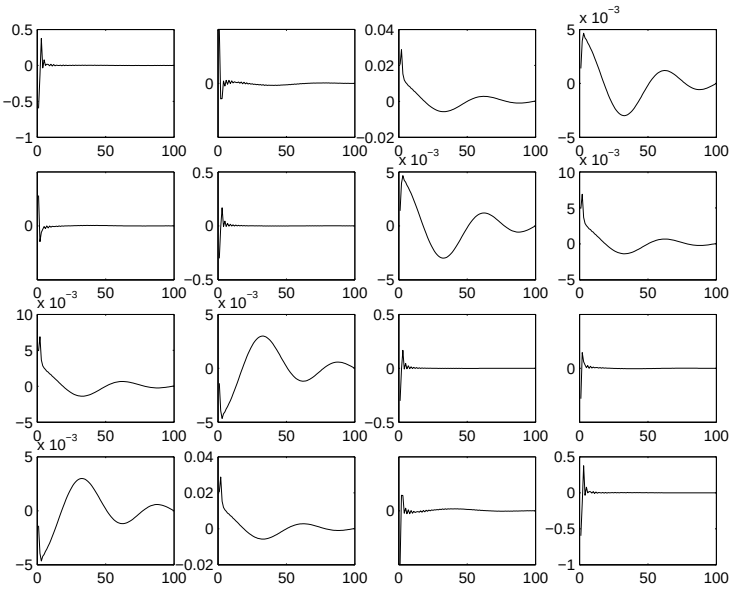

Fig. 6 Real parts of the summed convolution coefficients $\mathbf{S}^n_{k,l}$

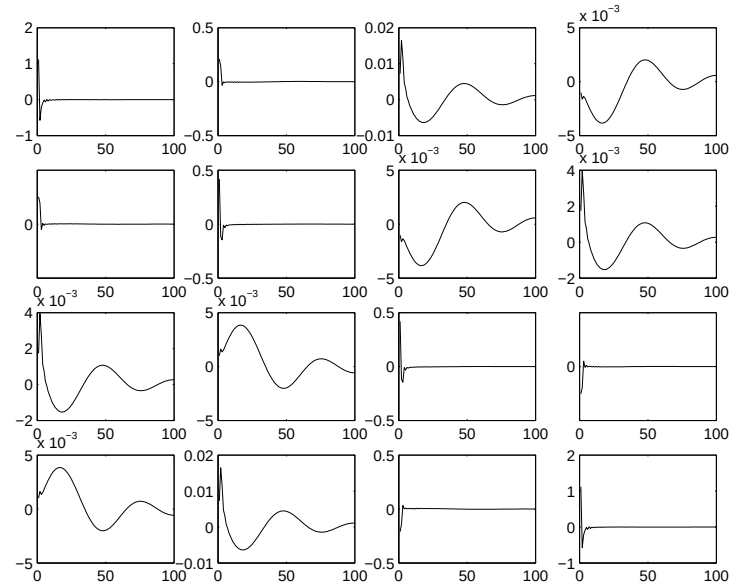

Fig. 7 Imaginary parts of the summed convolution coefficients $\mathbf{S}^n_{k,l}$

compromise between more smoothness of $\hat{\ell}\big|_{|z|=\rho}$ (which allows for an efficient discretisation of (29)), and growing instabilities for large ρ. This situation depending on the inversion radius is depicted in Fig. 8

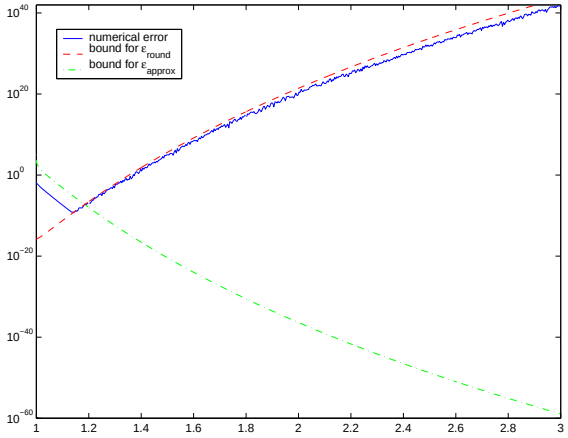

Fig. 8 Rounding and discretisation errors depending on the inversion radius.

For the numerical inverse transformation we choose a radius r and N equidistant sampling points $z_k = r\,e^{-ik2\pi/N}$. The approximate inverse transform,

$$\ell_n^N = \frac{1}{N} r^n \sum_{k=0}^{N-1} \hat{\ell}(z_k)\, e^{ink\frac{2\pi}{N}}, \quad n = 0, \dots N-1 \tag{30}$$

can then be calculated efficiently by an FFT. The numerical error of ℓ_n^N can be separated into ε_{approx}, the approximation error due to the finite number of sampling points, and the roundoff error ε_{round}, which is amplified by ρ^n. We refer the reader to [50] for more details and error estimates for this numerical inversion problem.

5 The Sum-of-Exponentials Approach and the Fast Evaluation of the Convolution

In order to reduce the numerical effort of the boundary convolutions (26), below that effort of the interior scheme, it is necessary to make some approximation. We will use the approach of Arnold, Ehrhardt and Sofronov [3] to approximate the coefficients $\widetilde{s}_{s,l}^n$ by the *sum-of-exponentials* ansatz and show a method to evaluate the discrete convolution with the approximated convolution coefficients $\widetilde{a}_{s,l}^n$ very efficiently. Afterwards we explain how these approximated convolution coefficients $\widetilde{a}_{s,l}^n$ enable us to evaluate the discrete convolution efficiently.

The sum-of-exponentials approximation has to be done for each element in $\mathbf{S}$ separately. We use for each $s, \tau = 1, \dots, d$ the following ansatz

$$\widetilde{s}^n_{s,\tau} \approx \widetilde{a}^n_{s,\tau} := \begin{cases} \widetilde{s}^n_{s,\tau}, & n = 0,\dots,\nu-1 \\ \sum\limits_{l=1}^{L(s,\tau)} b_{s,\tau,l}\, q_{s,\tau,l}^{-n}, & n = \nu,\nu+1,\dots \end{cases}, \tag{31}$$

where the number of summand in the approximation $L(s,\tau) \in \mathbb{N}$ and the starting index $\nu \geq 0$ (to disregard outliers) are tuneable parameters. The approximation quality of this sum-of-exponentials ansatz depends on $L(s,\tau)$, ν and the sets $\{b_{s,\tau,l}\}$ and $\{q_{s,\tau,l}\}$ for all $s,\tau = 1,\dots,d$.

Next we present the method to calculate these sets for given $L(s,\tau)$ and ν. We consider the formal power series

$$f_{s,\tau}(x) := \widetilde{s}^{\nu}_{s,\tau} + \widetilde{s}^{\nu+1}_{s,\tau} x + \widetilde{s}^{\nu+2}_{s,\tau} x^2 + \dots, \qquad \text{for } |x| \leq 1\,. \tag{32}$$

If the Padé approximation of (32)

$$\tilde{f}_{s,\tau}(x) := \frac{n^{(L(s,\tau)-1)}_{s,\tau}(x)}{d^{(L(s,\tau))}_{s,\tau}(x)}$$

exists (where the numerator and the denominator are polynomials of degree $L(s,\tau)-1$ and $L(s,\tau)$ respectively), then its Taylor series

$$\tilde{f}_{s,\tau}(x) = \widetilde{a}^{\nu}_{s,\tau} + \widetilde{a}^{\nu+1}_{s,\tau} x + \widetilde{a}^{\nu+2}_{s,\tau} x^2 + \dots$$

satisfies the conditions

$$\widetilde{a}^n_{s,\tau} = \widetilde{s}^n_{s,\tau} \quad \text{for} \quad n = \nu,\nu+1,\dots,2L(s,\tau)+\nu-1$$

according to the definition of the Padé approximation rule. In [3] Arnold, Ehrhardt and Sofronov showed how to compute the coefficient sets $\{b_{s,\tau,l}\}$ and $\{q_{s,\tau,l}\}$.

Theorem 3 ([3], Theorem 3.1.). *Let $d^{L(s,\tau)}_{s,\tau}$ have $L(s,\tau)$ simple roots $q_{s,\tau,l}$ with $|q_{s,\tau,l}| > 1$, $l = 1,\dots,L(s,\tau)$. Then*

$$\widetilde{a}^n_{s,\tau} = \sum_{l=1}^{L(s,\tau)} b_{s,\tau,l}\, q_{s,\tau,l}^{-n}\,, \qquad n = \nu,\nu+1,\dots,$$

where

$$b_{s,\tau,l} := -\frac{n^{(L(s,\tau)-1)}_{s,\tau}(q_{s,\tau,l})}{\left(d^{(L(s,\tau))}_{s,\tau}\right)'(q_{s,\tau,l})}\, q^{\nu-1}_{s,\tau,l} \neq 0\,, \qquad l = 1,\dots,L(s,\tau)\,.$$

The asymptotic decay of the $\widetilde{a}^n_{s,\tau}$ is exponential. This is due to the sum-of-exponentials ansatz (31) and the assumption $|q_{s,\tau,l}| > 1$, $l = 1,\dots,L(s,\tau)$.

If we use a $[L(s,\tau)-1|L(s,\tau)]$ Padé approximant to (32) then the first $2L(s,\tau)+\nu-1$ coefficients are reproduced exactly; however, the asymptotic behaviour of $\widetilde{s}^n_{s,\tau}$ and $\widetilde{a}^n_{s,\tau}$ (as $n \to \infty$) differs strongly (algebraic versus exponential decay).

We note that the Padé approximation must be performed with high precision ($2L(s,\tau)-1$ digits mantissa length) to avoid a 'nearly breakdown' by ill conditioned steps in the Lanczos algorithm (cf. [13]). If such problems still occur or if one root of the denominator is smaller than 1 in absolute value, the orders of the numerator and denominator polynomials are successively reduced. In our numerical test case we started with $L(s,\tau)\equiv 30$ and except from two outlier values the finally reached values of $L(s,\tau)$ were between 25 and 30. Fig. 9 shows the error $|\widetilde{s}^n_{s,\tau}-\widetilde{a}^n_{s,\tau}|$ versus n for the outlier with $L(1,2)=15$ for the imaginary part of $\widetilde{s}^n_{1,2}$ (a) and with $L(2,2)=30$ for the real part of $\widetilde{s}^n_{2,2}$ (b). The error increases significantly for $n>2L(s,\tau)+1$.

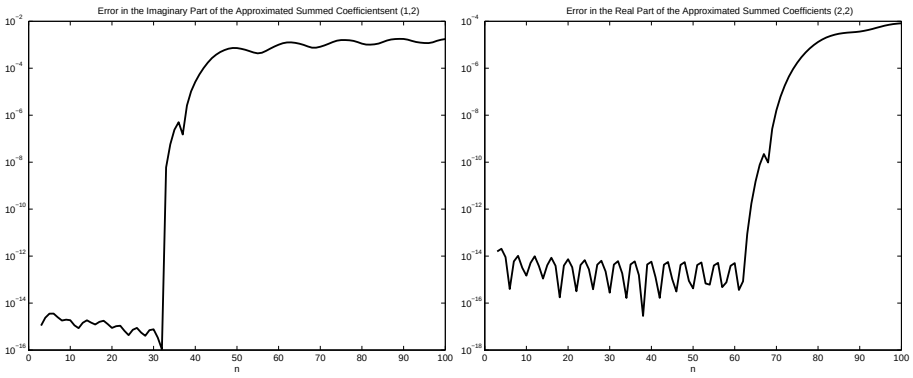

Fig. 9 Error $|\widetilde{s}^n_{s,\tau}-\widetilde{a}^n_{s,\tau}|$ versus n: imaginary part (a) for $s=1$, $\tau=2$ and (b) real part for $s=\tau=2$.

Now we describe the fast evaluation of the discrete approximate convolution

$$C^{(n+1)}_{s,\tau}(u) := \sum_{k=1}^{n+1-\nu} \widetilde{a}^{n+1-k}_{s,\tau}\, u^k_{\tau,J}\,, \quad \text{with } \widetilde{a}^n_{s,\tau} := \sum_{l=1}^{L(s,\tau)} b_{s,\tau,l}\, q^{-n}_{s,\tau,l}, \quad n=\nu,\nu+1,\dots$$

that can be calculated efficiently by a simple *recurrence formula*:

Theorem 4 ([3], Theorem 4.1.).

$$C^{(n+1)}_{s,\tau}(u) = \sum_{l=1}^{L(s,\tau)} C^{(n+1)}_{s,\tau,l}(u) \tag{33}$$

with

$$\begin{aligned} C^{(n+1)}_{s,\tau,l}(u) &= q^{-1}_{s,\tau,l} C^{(n)}_{s,\tau,l} + b_{s,\tau,l} q^{-\nu}_{s,\tau,l} u^{n+1-\nu}_{\tau,J}\,, \qquad n=\nu,\nu+1,\dots \\ C^{(\nu)}_{s,\tau,l}(u) &\equiv 0\,. \end{aligned} \tag{34}$$

This is an efficient and local-in-time approximation, that uses data only from ν levels earlier (typically $\nu=2$). Also, there is no need to store the boundary data, which becomes computationally expensive especially for higher dimensional problems.

Note that similar recursive convolution algorithms are successfully used in other applications as well, see [11] and references therein.

Let us summarize the proposed method to evaluate approximate discrete TBCs

1. For each s,τ choose $L(s,\tau)$ and ν and calculate the exact convolution coefficients $\widetilde{s}^n_{s,\tau}$ for $n = 0,\dots,2L(s,\tau)+\nu-1$.
2. For each s,τ use the Padé approximation for the Taylor series with $\widetilde{a}^n_{s,\tau} = \widetilde{s}^n_{s,\tau}$, for $n = \nu,\nu+1,\dots,2L(s,\tau)+\nu-1$ to calculate the sets $\{b_{s,\tau,l}\}$ and $\{q_{s,\tau,l}\}$ for all $s,\tau = 1,\dots,d$ according to Theorem 3.
3. Implement the recurrence formulas (33) and (34) to calculate the approximate convolutions.

6 Numerical Results

Finally we present the numerical results for simulating the time-dependent behaviour of the quantum well with the data of Section 1. We choose the time step $k = 0.015$ and the space step $h = 1/20$ for the computational domain $[-12,5]$ and compute the convolution coefficients of the discrete TBC as described in Section 5.

First, to study the behaviour of the discrete TBC, we consider a system of Schrödinger equations with potential set to zero ('free Schrödinger system'). As initial condition we use the Gaussian wave packet of heavy and light holes (4) stimulating a slow and a fast eigenmode. Fig. 10 shows the time-dependent behaviour of the first two components φ_1 (solid) and φ_2 (dashed). We focus on the first two components, since there is less mass in component three and four. The density oscillates between the components, moves to the right, fragments in two and the faster wave packet leaves the domain of computation without any visible reflections.

Secondly we consider only the faster mode and add the DBSQW structure (5), cf. Fig. 11. When the wave packet reaches the first barrier, it is partly reflected and partly transmitted. With advancing time some part of the density accumulates between the barriers and is slowly transmitted through the second barrier, then leaving the domain of computation. The part of the density, which is reflected at the first barrier moves on to the left and after some time most part of the solution leaves the computational domain in a packet. The wave packet does not recompose smoothly. A simulation for a slightly different DBSQW structure is shown in Fig. 12.

The *relative ℓ^2–error* is defined as

$$e_L(t) = \|\varphi - \varphi_a\|_2 / \|\varphi(.,0)\|_2,$$

where φ_a denotes the approximate solution obtained with the approximated discrete TBCs and φ is the solution calculated with exact discrete TBCs. When using the parameter $L(s,\tau) = 30$ initially in the sum-of-exponential approach (31) this relative ℓ^2–error increases moderately with respect to time (due to the interaction with the potential) but remains bounded after 1000 time steps below $6\cdot 10^{-3}$ which is acceptable for this application.

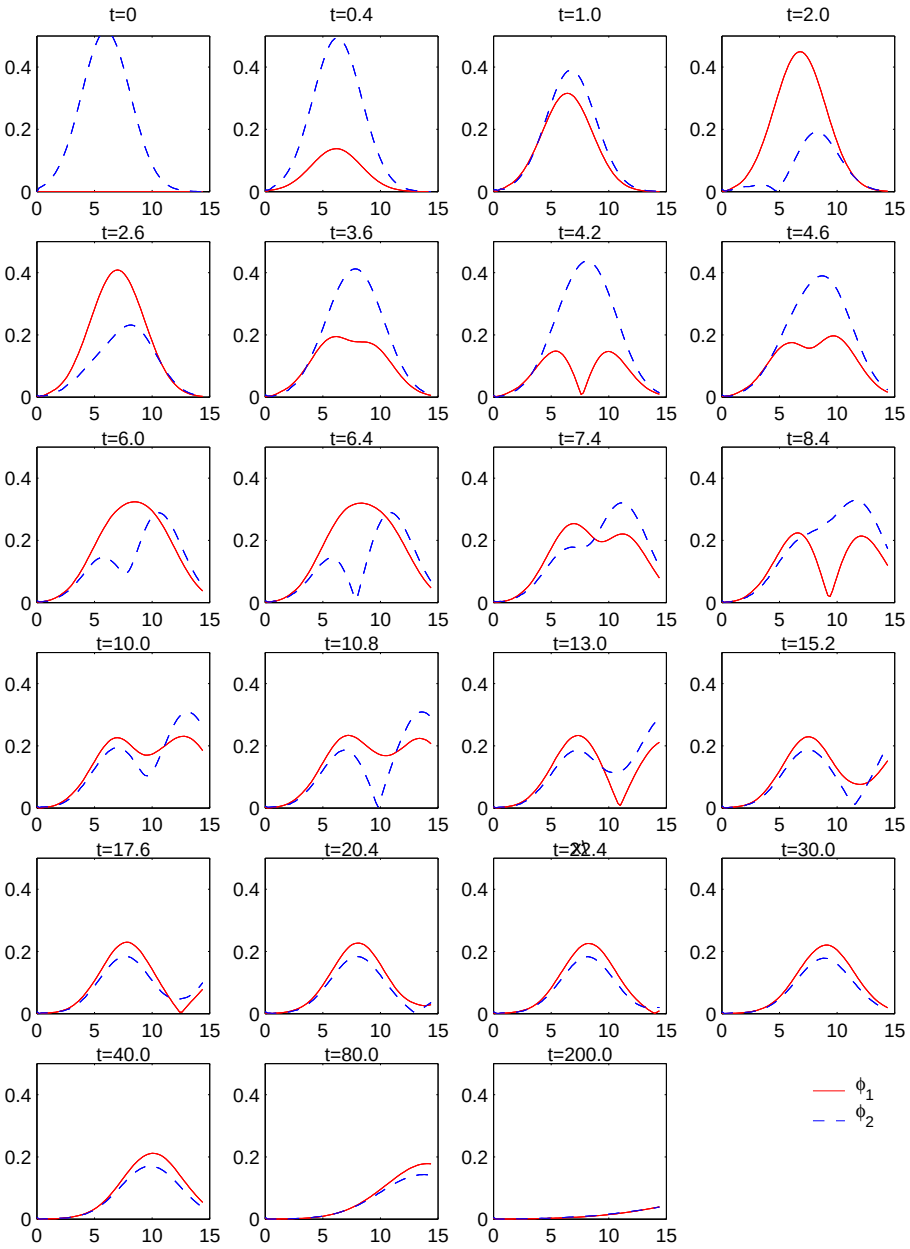

Fig. 10 Time dependent behaviour of φ_{1j} (solid) and φ_{2j} (dashed) for a free Schrödinger system.

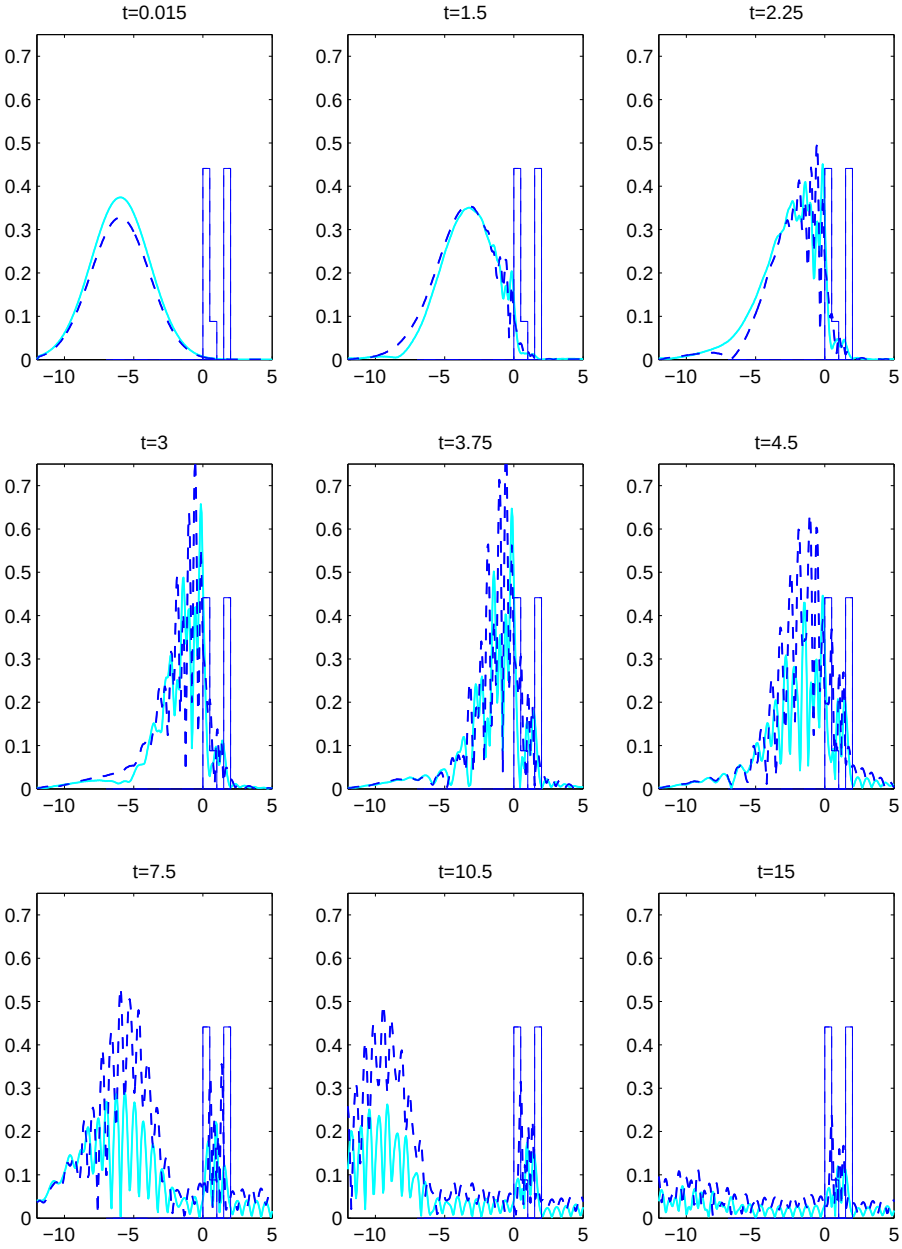

Fig. 11 Time dependent behaviour of φ_{1j} (solid) and φ_{2j} (dashed) for a system with DBSQW structure.

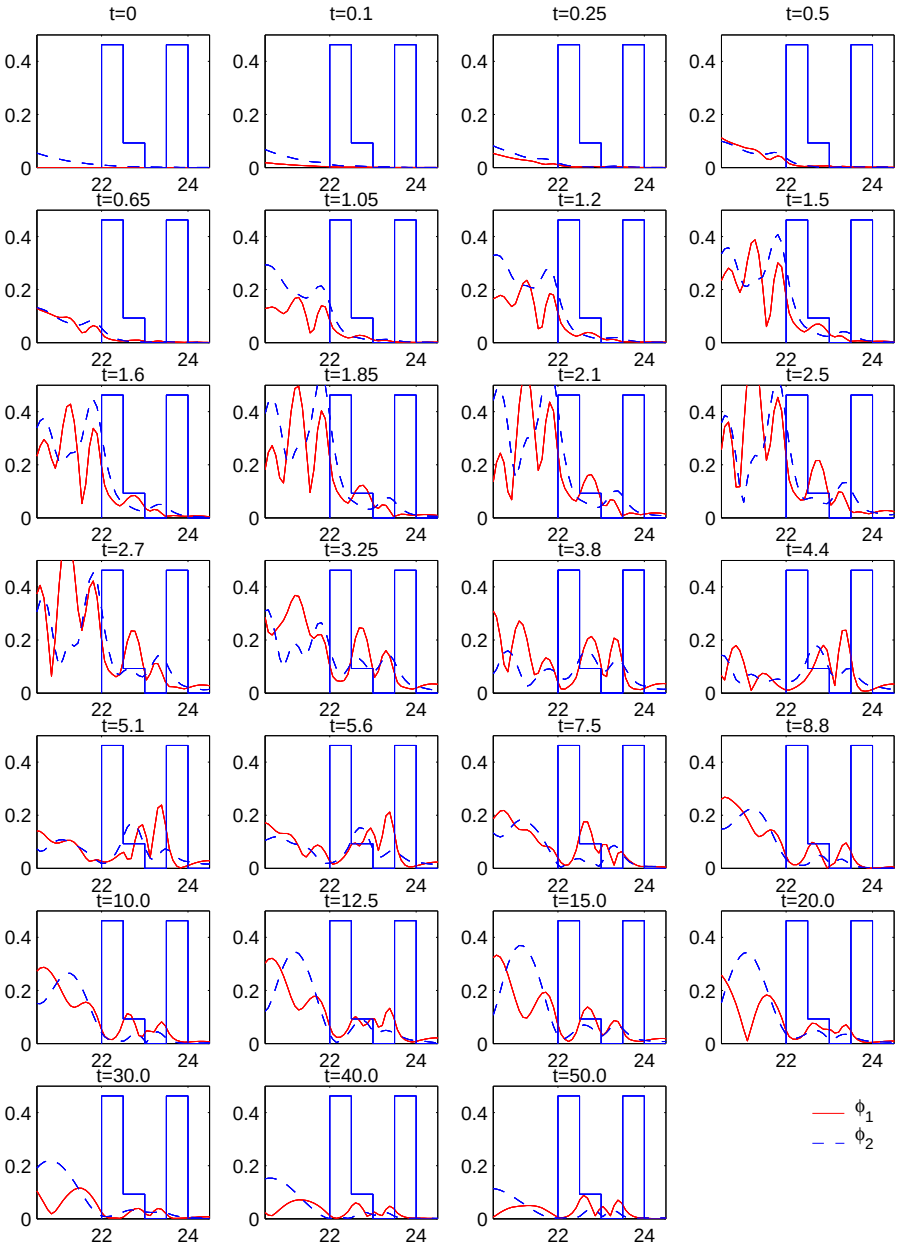

Fig. 12 Time dependent behaviour of φ_{1j} (solid) and φ_{2j} (dashed) for a different DBSQW system.

References

1. Antoine, A., Arnold, A., Besse, C., Ehrhardt, M., Schädle, A.: A Review of Transparent and Artificial Boundary Conditions Techniques for Linear and Nonlinear Schrödinger Equations. Commun. Comput. Phys. **4**, 729–796 (2008)
2. Arnold, A.: Numerically Absorbing Boundary Conditions for Quantum Evolution Equations. VLSI Design **6**, 313–319 (1998)
3. Arnold, A., Ehrhardt, M. Sofronov, I.: Discrete transparent boundary conditions for the Schrödinger equation: fast calculation, approximation, and stability. Commun. Math. Sci. **1**, 501–556 (2003)
4. Arnold, A., Ehrhardt, M., Schulte, M., Sofronov, I.: Discrete transparent boundary conditions for the Schrödinger equation on circular domains. Commun. Math. Sci. **10**, 889–916 (2012)
5. Bahder, T.B.: Eight-band $k \cdot p$ model of strained zincblende crystals. Phys. Rev. B **41**, 11992–12001 (1990)
6. Bastard, G.: Wave Mechanics Applied to Semiconductor Heterostructures. Hasted Press (1988)
7. Bandelow, U., Koprucki, T.: `WIAS-QW` for the simulation of strained multi quantum well structures. Online: http://www.wias-berlin.de/software/qw
8. Bandelow, U., Kaiser H.-C., Koprucki, T., Rehberg, J.: Spectral properties of $k \cdot p$ Schrödinger operators in one space dimension. Numer. Funct. Anal. Optim. **21**, 379–409 (2000)
9. Ben Abdallah, N., Kefi-Ferhane, J.: Mathematical Analysis of the two-band Schrödinger model. Math. Meth. Appl. Sci. **31**, 1131–1151 (2008)
10. Bittencourt, A.C.E., Cohen, A.M., Marques G.E.: Strain-induced enhancement of resonant current of holes in multilayered heterostructures. Phys. Rev. B **57**, 4525–4543 (1998)
11. Blakiewicz, G., Janke, W.: Recursive Convolution Algorithms for Time–Domain Simulation of Electronic Circuits. Comp. Meth. Sci. Techn. **7**, 91–109 (2001)
12. Borgioli G., Frosali G., Zweifel P.: Wigner approach to the two-band Kane model for a tunneling diode. Transp. Theory Stat. Phys. **32**, 347–366 (2003)
13. Bultheel, A., Van Barel, M.: Linear algebra, rational approximation and orthogonal polynomials. Studies in Computational Mathematics 6, North–Holland (1997)
14. Burt, M.G.: The justification for applying the effective-mass approximation to microstructures. J. Phys. Condens. Matter **4**, 6651–6690 (1992)
15. Burt, M.G.: Direct derivation of effective-mass equations for microstructures with atomically abrupt boundaries. J. Phys. Condens. Matter **11**, R53–R83 (1998)
16. Cardona, M.: Fundamentals of Semiconductors. Springer, Berlin (1996)
17. Chao, C.Y.-P., Chuang, S.L.: Spin-orbit-coupling effects on the valence-band structure of strained semiconductor quantum wells. Phys. Rev. B **46**, 4110–4122 (1992)
18. Chuang, S.L.: Efficient band-structure calculations of strained quantum wells. Phys. Rev. B **43**, 9649–9661 (1991)
19. Chuang, S.L.: Physics of Optoelectronic Devices. Wiley & Sons, New York (1995)
20. Debernardi, P., Fasano, P.: Quantum confined Stark effect in semiconductor quantum wells including valence band mixing and Coulomb effects. IEEE J. Quant. Electron. **29**, 2741–2755 (1993)
21. Ehrhardt, M.: Discrete artificial boundary conditions. PhD, Technische Universität Berlin (2001)
22. Ehrhardt, M., Arnold, A.: Discrete transparent boundary conditions for the Schrödinger equation. Riv. Matem. Univ. di Parma **6**, 57–108 (2001)
23. Ehrhardt, M.: Discrete Transparent Boundary Conditions for Schrödinger-type equations for non-compactly supported initial data, Appl. Numer. Math. **58**, 660–673 (2008)
24. Enders, P., Woerner, M.: Exact 4×4 block diagonalization of the eight-band $k \cdot p$ Hamiltonian matrix for tetrahedral semiconductors and its application to strained quantum wells. Semicond. Sci. Technol. **11**, 983–988 (1996)
25. Franceschetti, A., Wei, S.-H., Zunger, A.: Effects of ordering on the electron effective mass and strain deformation potential in $GaInP_2$: Deficencies of the $k \cdot p$ model. Phys. Rev. B **52**, 992–997 (1995)

26. Kane, E.O.: Energy Band Theory. in Paul, W. (ed.): Handbook on Semiconductors. North-Holland, Amsterdam, New York, Oxford (1982)
27. Kefi, J.: Analyse mathématique et numérique due modèles quantiques pour les semiconducteurs. PhD. Université Toulouse III - Paul Sabatier (2003)
28. Kisin, M.V., Gelmont, B.L., Luryi, S.: Boundary-condition problem in the Kane model. Phys. Rev. B **58**, 4605–4616 (1998)
29. Klindworth, D.: Discrete Transparent Boundary Conditions for Multiband Effective Mass Approximations. Diploma Thesis, Technische Universität Berlin (2009)
30. Koprucki, T., Baro, M. Bandelow, U., Tien, T.Q., Weik, F., Tomm, J.W., Grau M., Amann, M.-Ch.: Electronic structure and optoelectronic properties of strained InAsSb/GaSb multiple quantum wells. Appl. Phys. Lett. **87**, 81911/1–181911/3 (2005)
31. Koprucki, T., Kaiser, H.-C., Fuhrmann, J.: Modeling and simulation of strained quantum wells in semiconductor lasers. In: Mielke, A. (ed.): Analysis, Modeling and Simulation of Multiscale Problems, Springer, Heidelberg, pp. 365–394 (2006)
32. Koprucki, T.: On $k \cdot p$-Schrödinger Operators. PhD, Freie Universität Berlin (2008)
33. Lake R., Klimeck G., Bowen R.C., Jovanovic D.: Single and multiband modeling of quantum electron transport through layered semiconductor devices. J. Appl. Phys. **81**, 7845–7869 (1997)
34. Liu, Y.X, Ting, D.Z.-Y., McGill, T.C.: Efficient, numerically stable multiband $k \cdot p$ treatment of quantum transport in semiconductor heterostructures. Phys. Rev. B **54**, 5675–5683 (1996)
35. Luttinger J.M., Kohn W.: Motion of electrons and holes in perturbed periodic fields. Phys. Rev. **94**, 869–883 (1955)
36. Meney, A.T., Gonul, B., O'Reilly, E.P.: Evaluation of various approximations used in the envelope-function method. Phys. Rev. B **50**, 10893–10904 (1994)
37. Pokatilov, E.P., Fonoberov, V.A., Fomin, V.M., Devreese, J.T.: Development of an eight-band theory for quantum dot heterostructures. Phys. Rev. B, **64**, 245328, (2001)
38. Rodina, A.V., Alekseev, A.Y., Efros, A.L., Rosen, M., Meyer, B.K.: General boundary conditions for the envelope function in the multiband $k \cdot p$ model. Phys. Rev. B **65**, 125302 (2002)
39. Sankaran, V., Singh, J.: Formalism for tunneling of mixed-symmetry electronic states: Application to electron and hole tunneling in direct- and indirect-band-gap GaAs/Al_xGa_{1-x}As structures. Phys. Rev. B **44**, 3175–3186 (1991)
40. Singh, J.: Physics of semiconductors and their heterostructures. McGraw-Hill, New York (1993)
41. Sirtori, C., Kruck, P., Barbieri, S., Collot, Ph., Nagle, J., Beck, M., Faist, J., Oesterle, U.: GaAs/Al_xGa_{1-x}As quanstum cascade lasers. Appl. Phys. Lett. **73**, 3486–3488 (1998)
42. Söderström J.R., Yu E.T., Jackson M.K., Rajakarunanayake Y., McGill T.C.: Two-band modeling of narrow band gap and interband tunneling devices. J. Appl. Phys. **68**, 1372–1375 (1990)
43. Stovneng, J.A., Hauge, E.H.: Time-dependent resonant tunneling of wave packets in the tight-binding model. Phys. Rev. B **44**, 13582–13594 (1991)
44. Sweeny M., Xu J.: Resonant interband tunnel diodes. Appl. Phys. Lett. **54** 546–548 (1989)
45. Veprek, R.G., Steiger, S., Witzigmann, B.: Ellipticity and the spurious solution problem of $k \cdot p$ envelope equations. Phys. Rev. B **76**, 165320 (2007)
46. Wagner, M., Mizuta, H.: Complex-energy analysis of intrinsic lifetimes of resonances in biased multiple quantum wells. Phys. Rev. B **48**, 14393–14406 (1993)
47. Wood, D.M., Zunger, A.: Successes and failures of the $k \cdot p$ method: A direct assessment for GaAs/AlAs quantum structures. Phys. Rev. B **53**, 7949–7963 (1996)
48. Zhang, J., Gu, B.: Temporal characteristics of electron tunneling in double-barrier stepped quantum-well structures. Phys. Rev. B **43**, 5028–5034 (1991).
49. Zisowsky, A.: Discrete transparent boundary conditions for systems of evolution equations. PhD, Technische Universität Berlin (2003)
50. Zisowsky, A., Arnold, A., Ehrhardt, M., Koprucki, T.: Discrete transparent boundary conditions for transient $k \cdot p$-Schrödinger equations with application to quantum heterostructures. Z. Angew. Math. Mech. **85**, 793–805 (2005)